Supporting Online Material

The high affinity *E. coli* methionine ABC transporter: structure and allosteric regulation

Neena S. Kadaba, Jens Kaiser, Eric Johnson, Allen Lee and Douglas C. Rees

Cloning and Expression

MetNI Following a similar strategy used in the BtuCD and HI1470/71 structure determinations (*S1, S2*), *metN* and *MetI* were cloned from *E. coli* K-12 genomic DNA (American Type Culture Collection) into a modified fusion pET21b(+)/pET19b vector that can co-express the *metI* and *metN* genes simultaneously using separate T7 promoters. The entire *metNIQ* operon was isolated from the genomic DNA by PCR and inserted into a pCR-Blunt II-TOPO vector (Invitrogen). The *metN* (ATPase subunit) gene was subsequently isolated by PCR using two oligonucleotides which inserted NdeI and XhoI sites. The PCR fragment was ligated into a pET19b vector (Novagen/EMD) using the NdeI and XhoI sites to introduce an N-terminal 10x histidine tag. Similarly, the *metI* (transmembrane subunit) gene was isolated by PCR using two oligonucleotides which inserted NdeI and XhoI sites and removed the STOP codon from the end of the gene. The PCR fragment was ligated into a pET21b(+) vector (Novagen/EMD) using the NdeI and XhoI sites to introduce a C-terminal 6x histidine tag.

The *metI* gene was isolated by PCR using the *metI*-pET21b(+) plasmid as the template with two oligonucleotides designed to anneal upstream and downstream of the entire promoter/expression region of the pET21b(+) plasmid, and introduce SphI and BglII sites at the ends of the PCR product. This PCR fragment was digested with SphI and BglII and ligated into the *metN*-pET19b vector. The SphI and BglII sites in the *metN*-pET19b vector are located in a non-coding region of the pET19b plasmid. The modified pET19b vector can express the *metI* and *metN* genes simultaneously using separate T7 promoters. A mutagenesis reaction was then performed on the *metNI*-pET19b plasmid to insert a STOP codon immediately after the *metI* gene so that the C-terminal 6x histidine tag will not be expressed. The reaction was performed using the Quickchange Mutagenesis Kit (Stratagene). As a result, the final plasmid contains an ATPase subunit with an N-terminal MGHHHHHHHHHHSSGHIDDDDKH sequence, while the transmembrane subunit has no additional residues.

The cloned plasmid was transformed into BL21-gold (λDE3) cells (Novagen/EMD) and protein expression was carried out at 37 ˚C in Terrific Broth with 0.2 mg/mL ampicillin and 1% glucose instead of glycerol. The cells were induced at OD 600 nm = 4.0 with 2 mM IPTG for 2 hours and then stored at -80 ˚C.

ΔC2-MetNI, and MetNI E166Q constructs Mutagenesis reactions were performed on the final *metNI*-expression plasmid to insert a STOP codon immediately after the *metN* sequence encoding V225, or to replace the *metN* sequence encoding E166 with a sequence encoding Q166, to create the ΔC2-MetNI, and MetNI E166Q constructs, respectively. The reactions were performed using the Quickchange Mutagenesis Kit (Stratagene). As a result, the final plasmids are identical to the final *metNI*-expression plasmid except for the changes introduced by the site directed mutagenesis described above.

MetN-C2 The *metN-C2* construct, encoding the C-terminal 100 amino acids of MetN followed by a 6x histidine tag (Met-L247-E347-6xH), was created by PCR amplification using the *metN*-pET19b plasmid as template and the oligonucleotides:
5'-CACCTATACATATGCTGGATATCCCGGAGGATTACCAGGAACGTC-3' and
5'-CACATCATCCTCGAGGACATAACCCAGTACCTCTA-3'.
PCR product and pET 19b vector were NdeI, XhoI digested and subsequently ligated to yield the *metN-C2* plasmid. The *metN-C2* plasmid was transformed into BL21-gold (λDE3) cells (Novagen/EMD) and protein expression was carried out at 37 ˚C in Terrific Broth containing 0.5% glycerol and 0.1 mg/mL ampicillin in 6L flasks. Three hours of target gene expression was induced by the addition of IPTG to a final concentration of 1 mM. Cells were cooled in an ice slurry and harvested via centrifugation at 4 ˚C before freezing at -80 ˚C.

Purification and Crystallization

MetNI 10 gm of cell paste were suspended in 50 mL of 50 mM TrisHCl, pH7.5, 20 mM imidazole, 1 M NaCl solution with 40 mL added water. The suspension was homogenized, after which 10 mL of a 10% n-dodecyl-β-D-maltopyranoside (DDM, Anatrace) solution and a protease inhibitor tablet (Roche) was added, bringing the final concentration to 1% DDM. The 100 mL solution was split into two solutions of 50 mL each and placed on ice. Each of these solutions was sonicated using a program that allowed for 0.5 seconds on, followed by 1.5 seconds off, in one minute increments. The two solutions were alternatively sonicated for one minute each, until each solution was sonicated for a total of 4 minutes. After sonication, the solutions were re-combined and stirred for 1 hour at 4 ˚C before centrifugation at 39,700 xg for 30 minutes. The supernatant was loaded and equilibrated onto a 5 ml Ni-sepharose affinity chromatography column (GE Healthcare), washed with 92 mM imidazole, and eluted with 250 mM imidazole, 25 mM Tris HCl, pH 7.5, 500 mM NaCl, and 0.1% DDM. The eluate was dialyzed overnight into a solution containing 0.1% DDM, 25 mM Tris 7.5, 500 mM NaCl, 5 mM dithiothreitol, 2.5 mM $MgCl_2$ and 2.5 mM ATP before concentrating to 20 mg/ml in Amicon Ultra 15 centrifugal concentrators (Millipore) with a 100 kDa molecular weight cutoff. Protein purity was estimated to be greater than 90% using SDS gel electrophoresis.

Crystallization experiments were carried out with the hanging drop method at 20 ˚C, using 2 μL protein plus 2 μL precipitant solution. Chunky, diamond shaped crystals were obtained using solutions in the range of 28-32% PEG 400, 0.05 M Li_2SO_4, 0.2 M $(NH_4)_2HPO_4$, 0.05-0.15 M $(NH_2)_2SO_4$, and 0.1 M sodium citrate pH 4.2-4.5. Crystals grew to 0.3 x 0.3 x 0.4 mm^3 in two to three weeks, and were frozen in liquid nitrogen prior to data collection.

Selenomethionine substituted protein was made using *E. coli* B834 (DE3) cells (EMD Biosciences) grown in M9 medium supplemented with seleno-D,L-methionine. Procedures for purification and crystallization of the selenomethionine substituted protein were identical to that of the native protein.

Xenon-derivatized crystals were prepared by pressurizing native crystals to 100 psi Xe gas for 10 minutes in a pressure chamber. Selenomethionine-soaked crystals were obtained by soaking native crystals in 1mM to 20mM L-selenomethionine for 30 minute to 3 hours.

MetN-C2 Ten grams of frozen cell pellet were resuspended in 75 ml of ice cold lysis buffer (50 mM TAPS, 250 mM NaCl, pH 7.7, DNase and lysozyme each at 10 μg/ml). Cell lysis was performed at 4 ˚C by repeated passage (4x) of the cell suspension through a M-110L microfluidizer processor (Microfluidics), followed by addition of ice cold lysis buffer to reach a total volume of 100 ml. Clearing of cell lysates was performed by centrifugation at 30K xg, 40 minutes, 4 ˚C. Cleared lysates containing 50 mM imidazole were then loaded to a 5 ml Ni-sepharose HP column (GE Healthcare) equilibrated with 95% buffer A (50 mM TAPS, 250 mM NaCl, pH 7.7) and 5% buffer B (50 mM TAPS, 250 mM NaCl, 1 M imidazole, pH 7.7). The column was washed with 10 column volumes 9% buffer B, and the target protein was eluted by stepping to 50% buffer B. Buffer exchange and protein concentration were performed in Amicon Ultra 15 centrifugal concentrators (Millipore) with a 5 kDa molecular weight cutoff. Protein purity was estimated to be ≥ 95% via SDS-PAGE.

Initial protein crystals were formed after 48 hours at 20 ˚C using the sitting drop vapor diffusion method in 96 well plates. The crystallization drops contained a mixture of 300 nl purified MetN-C2 protein (30 mg/ml) and 300 nl 0.1 M bis-trisHCl, pH 5.5, 2 M ammonium sulfate. Optimization of crystallization conditions (2.35 μl purified protein (30 mg/ml) mixed with 2.65 μl 50 mM bis-tris, pH 5.5, 1.8 M ammonium sulfate, and 15% glycerol) resulted in the formation of single hexagonal crystals having dimensions of approximately 0.6 x 0.5 x 0.4 mm^3 after incubation for 48 hours at 20 ˚C. Potassium iodide derivatives were prepared by soaking native crystals in a 20 μl drop of solution containing 50 mM bis-trisHCl, pH 5.5, 1.8 M ammonium sulfate, 15% glycerol and 0.5 M KI for 5 minutes at 25 ˚C.

Protein Purification for ATPase assays: wt, E166Q and ΔC2 MetIN mutants

Ten grams of frozen cell pellet were resuspended in 75 ml of ice cold lysis buffer (50 mM TAPS, 250 mM NaCl, pH 8.5, DNase and lysozyme each at 10 μg/ml). Cell lysis was performed at 4 ˚C by repeated passage (4x) of the cell suspension through a M-110L microfluidizer processor (Microfluidics), followed by addition of 1 gm DDM and ice cold lysis buffer to reach 1% DDM and a total volume of 100 ml. Detergent extraction proceeded with stirring at 4 ˚C for 1 hr. Clearing of the extract was then performed by centrifugation at 30K xg, for 40 min at 4 ˚C. The cleared extracts containing 50 mM imidazole were then loaded to a 5 ml Ni-sepharose HP column (GE Healthcare) equilibrated with 95% buffer A (50 mM TAPS, 250 mM NaCl, pH 8.5, and 0.05% DDM) and 5% buffer B (50 mM TAPS, 250 mM NaCl, 1 M imidazole, pH 8.5, and 0.05% DDM). The column was washed with 10 column volumes 9% buffer B, and the target protein was eluted by stepping to 50% buffer B. Buffer exchange and protein concentration were performed in Amicon Ultra 15 centrifugal concentrators (Millipore) with a 100 kDa molecular weight cutoff. Protein purity was estimated to be ≥ 90% via SDS-PAGE. The protein was concentrated to approximately 5 mg/ml followed by addition of glycerol to 10%, and flash freezing on liquid nitrogen.

Data Collection and Structure Determination.

Data collection and refinement statistics for the MetNI and MetN-C2 structures are provided in Tables S1 and S2, respectively.

MetNI A 3.7 Å resolution native dataset was collected at the Stanford Synchrotron Radiation Laboratory (SSRL) beam line 11-1 and processed using MOSFLM (*S3*) and SCALA of the

CCP4 program suite (*S4*). A 3.7 Å resolution Xenon-derivatized dataset (1.5 Å wavelength) was collected at the Stanford Synchrotron Radiation Laboratory beam line 9-2 and processed using MOSFLM and SCALA. A 3-wavelength, 6.5 Å resolution dataset using selenomethionine-substituted crystals was collected at the Advanced Light Source beam line 8.2.1 and processed using MOSFLM and SCALA (only the peak data set was used in the crystal structure determination). A peak wavelength, 5.22 Å resolution dataset of a crystal soaked in 1 mM L-selenomethionine for 2 hours was collected at SSRL beam line 9-2 and processed using MOSFLM and SCALA. As assessed by the UCLA Diffraction Anisotropy Server (http://www.doe-mbi.ucla.edu/~sawaya/anisoscale (*S5*)) and during refinement, the MetNI diffraction data exhibited pronounced anisotropy, characterized with an overall anisotropic thermal ellipsoid with components B_{11} ~ -26 Å^2, B_{22} ~ +67 Å^2, B_{33} ~ -41 Å^2 (ie, the weakest and strongest directions of the diffraction pattern correspond to the b and c axes, respectively.)

The xenon binding sites were found by the program SHELX (*S6*) using the single wavelength anomalous diffraction (SAD) data collected from a xenon pressurized crystal, and single isomorphous replacement and anomalous scattering phases were refined through solvent flattening and histogram matching using SHARP (*S7*), and four-fold noncrystallographic symmetry averaging with MAIN (*S8*) and DM (*S9*). The electron density map averaged with the final, refined operators is illustrated in Figure S1. Manual building was done in COOT (*S10*) and MAIN (*S8*), facilitated by the location of the selenomethionine positions in the selenomethionine incorporated crystals (after molecular replacement with an early model using MOLREP (*S11*) to compensate for the non-isomorphism between the two crystal forms) and the 2.1 Å resolution structure of the isolated MetN-C2 domain (below). Refinement was carried out using CNS (v1.2; (*S12*), using Ramachandran potentials), MAIN ((*S8*), using manually defined hydrogen bond restraints), and REFMAC (*S13*).

The binding sites for selenomethionine soaked into MetNI crystals (1 mM for two hours) were established by anomalous difference Fourier maps calculated with data collected at the selenium peak and model phases. Selenomethionine was only observed to bind to the C2-domains; no binding sites were found within the translocation pathway, so that an occluded ligand binding site as observed in the maltose transporter structure (*S14*) is not present. Following refinement to correct for slight changes in transporter orientation in the crystals, residues surrounding the binding site are depicted in Figure S2.

MetN-C2 Data for the potassium iodide derivative extended to approximately 2.0 Å resolution and was collected to 2.1 Å resolution on a in-house source. Data processing used MOSFLM (*S3*) and SCALA programs of the CCP4 suite (I*4*). Initial phases and heavy atom binding sites were determined from SAD data by the program SHELX (*S6*). Automated model building was performed using ARP/wARP (*S15*) followed by manual building using COOT (*S10*) and MAIN (*S8*). REFMAC (*S13*) was used for model refinement, and solvent atoms were located using the ARP option in REFMAC. The *E. coli* MetN-C2 domain is homologous to the RCSB Protein Data Bank (PDB; (*S16*)) entries 2QSW and 2QPR.

Attempts to obtain methionine bound crystals of MetN-C2 by either cocrystallization or soaking approaches were unsuccessful.

Activity Assays

ATPase activity assays of the wt, E166Q, and ΔC2 mutants of MetNI were performed using the EnzChek™ phosphate assay kit (Molecular Probes, Eugene, OR). Assays were performed in a Infinite 200 microplate reader (Tecan) with the temperature controlled at 37 ˚C. The assay uses the method of Webb (*S17*) that monitors the release of free phosphate by coupling the phosphatase reaction with the enzymatic conversion of 2-amino-6-mercapto-7-methyl-purine riboside to 2 amino-6-mercapto-7-methyl purine and ribose-1-phosphate by purine nucleoside phosphorylase. The substrate 2-amino-6-mercapto-7-methyl-purine riboside has an absorbance maximum of 330 nm, whereas the maximum absorption of the product is 360 nm. Each 110 μl reaction mixture contained 50 mM TrisHCl, pH 7.5, 200 μM 2-amino-6-mercapto-7-methyl-purine riboside, 1 unit of purine nucleoside phosphorylase, 0.05% DDM, 200 μM EDTA, 1 mM ATP, D-, L, or selenomethionine at 0, 15, 30, 50, 100, or 200 μM, and 1.1 μM of the wt, E166Q, or ΔC2 MetIN preparation. Reactions were monitored at 360 nm for 2 minutes before initiation of the reaction by automatic injection of Mg^{2+} to a final concentration of 2 mM. Initial reaction velocities were determined using the Magellan software by calculating the mean slope of linear data points following injection of Mg^{2+}. The specific activity and K_m for ATP in this ATPase assay were estimated to be 300 nmoles Pi/min/mg transporter (equivalent to ~40 moles Pi/min/mole transporter) and ~300 μM, respectively (Figure S3).

Structural comparisons

Residues in the transmembrane helices of MetI are assigned TM1, 5-40; TM2, 52-65 (with a kink at Pro67 leading to a helix from 69-81; TM3, 89-114 (with a kink at 102); TM4, 146-163 (with a kink at 155); TM5, 188-209.

The initial comparisons between the molybdate ModBC ((*S18*); PDB 2ONK), maltose MalFGK ((*S14*), PDB 2R6G) and methionine transporter structures were performed with SUPERPOSE (*S19*). These superpositions were used to calculate overall root mean square deviations (rmsds), and to identify structurally conserved elements that were then superimposed using a program based on an algorithm of Kabsch (*S20*). For these comparisons, structurally conserved elements were used that approximately corresponded to TM2, TM3 and TM4 of the methionine transporter, specifically MetI residues 48-79 and 101-160; ModB residues 79-110 and 140-199; MalF residues 309-340 and 381-440; and MalG residues 113-144 and 170-229. A more complete structure based alignment of the membrane spanning subunits MetI, ModB and MalFG, derived using the MUSTANG multiple structural alignment algorithm (*S21*), is provided in Figure S4.

Structurally conserved elements of the β-sheet in the ABC subunit catalytic domain consist of MetN residues 3-10, 24-30, 32-50, 60-65, 83-89, 160-166, 192-198, 210-216 and 220-224; ModC residues 4-11, 18-43, 53-58, 71-77, 146-152, 178-184, 196-202, 206-210; and MalK residues 5-12, 22-28, 30-48, 58-63, 76-82, 153-159, 185-191, 203-209 and 213-217.

The structures of the maltose, molybdate and methionine transporters represent a progression of inward facing conformations of the translocation pathway that range from closed to wide open, respectively (Figure S5). To characterize the relationships between these conformations, the rigid body transformations relating these structures were calculated (*S20*) using structurally conserved residues in the membrane spanning subunits (corresponding to TM2, TM3 and TM4

of MetI) and using the structurally conserved β-sheet in the NBDs. For the reference state, the appropriate residues of the molybdate and methionine transporters were superimposed onto the MalF subunit of the maltose transporter. The transformations required to superimpose the appropriate helices of MalG with the corresponding regions of ModB and MetI are equivalent to rigid body rotations of ~22˚ and 32˚, respectively. These rotation angles provide a measure of the quaternary structure changes associated with the increased opening of the translocation pathway progressing from the closed state in MalFGK, to the inward facing state of ModBC and the widely separated methionine transporter. To extract the basic elements of these transformations, a principal components analysis (*S22*) was conducted to identify the major contribution to the relationship between these structures. The rotation axes that dominate the interconversion of the membrane spanning subunits and the interconversion of the NBDs are both approximately perpendicular to the symmetry axis of the reference maltose transporter and pass near through the conserved proline (Pro 67 in MetI) at the kink in TM2 near the periplasmic surface, and the cytoplasmic coupling helices between TM3 and TM4, respectively.

References

S1. K. P. Locher, A. T. Lee, D. C. Rees, *Science* **296**, 1091 (2002).
S2. H. W. Pinkett, A. T. Lee, P. Lum, K. P. Locher, D. C. Rees, *Science* **315**, 373 (2007).
S3. A. G. W. Leslie, *Joint CCP4 and ESF-EACBM Newsletter on Protein Crystallography* (1992).
S4. Collaborative Computational Project No 4, *Acta crystallogr.* **D50**, 760 (1994).
S5. M. Strong *et al.*, *Proc. Natl. Acad. Sci. USA* **103**, 8060 (2006).
S6. T. R. Schneider, G. M. Sheldrick, *Acta crystallogr.* **D58**, 1772 (2002).
S7. G. Bricogne, C. Vonrhein, C. Flensburg, M. Schiltz, W. Paciorek, *Acta crystallogr.* **D59**, 2023 (2003).
S8. D. Turk, in *Methods in Macromolecular Crystallography, NATO Science Series I* D. Turk, L. Johnnson, Eds. (IOS Press, 2001), vol. 325, pp. 148-155.
S9. K. Cowtan, *Joint CCP4 and ESF-EACBM Newletter on Protein Crystallography* **31**, 34 (1994).
S10. P. Emsley, K. Cowtan, *Acta crystallogr.* **D60**, 2126 (2004).
S11. A. Vagin, A. Teplyakov, *J. Appl. Cryst.* **30**, 1022 (1997).
S12. A. T. Brunger, *Nature Protocols* **2**, 2728 (2007).
S13. G. N. Murschudov, A. A. Vagin, E. J. Dodson, *Acta crystallogr.* **D53**, 240 (1996).
S14. M. L. Oldham, D. Khare, F. A. Quiocho, A. L. Davidson, J. Chen, *Nature* **450**, 515 (2007).
S15. A. Perrakis, R. Morris, V. S. Lamzin, *Nature Str. Mol. Biol.* **6**, 458 (1999).
S16. H. M. Berman *et al.*, *Nuc. Acids Res.* **28**, 235 (2000).
S17. M. R. Webb, *Proc. Natl. Acad. Sci. USA* **89**, 4884 (1992).
S18. K. Hollenstein, D. C. Frei, K. P. Locher, *Nature* **446**, 213 (2007).
S19. E. Krissinel, K. Henrick, *Acta crystallogr.* **D60**, 2256 (2004).
S20. W. Kabsch, *Acta crystallogr.* **A32**, 922 (1976).
S21. A. S. Konagurthu, J. C. Whisstock, P. J. Stuckey, A. M. Lesk, *Proteins Struct., Funct., Gen.* **64**, 559 (2006).
S22. A. Amadei, A. B. M. Linssen, H. J. C. Berendsen, *Proteins Struct., Funct., Gen.* **17**, 412 (1993).
S23. M. S. Weiss, *J. Appl. Cryst.* **34**, 130 (2001).
S24. R. A. Laskowski, M. W. MacArthur, D. S. Moss, J. M. Thornton, *J. Appl. Cryst.* **26**, 283 (1993).
S25. P. J. Kraulis, *J. Appl. Crystallogr.* **24**, 946 (1991).
S26. E. A. Merritt, M. E. P. Murphy, *Acta crystallogr.* **D50**, 869 (1994).

Table S1: Data Processing, Phasing and Refinement Statistics for native, xenon-pressurized, selenomethionine incorporated and selenomethionine soaked MetNI crystals

Data Processing Statistics	**Native**	**Xenon**	**SeMet peak**	**SeMet soak**
unit cell dimensions (a,b,c) (space group $P2_12_12_1$, with two MetNI tetramers per asymmetric unit)	97.70 Å 165.40 Å 289.02 Å	97.68 Å 169.02 Å 290.38 Å	93.79 Å 159.59 Å 294.33 Å	99.77 Å 164.06 Å 292.00 Å
wavelength (Å)	1.00[e]	1.5[f]	0.97960[g]	0.97901[f]
[a]resolution (Å)	44.6-3.7 (3.9-3.7)	45 – 3.7 (3.9-3.7)	40-6.5 (6.85-6.5)	47.7-5.22 (5.50-5.22)
unique reflections	50,082 (6,581)	50,662 (6,071)	9,197 (1,334)	15,956 (1,272)
redundancy	13.6 (9.9)	7.5 (4.9)	12.1 (11.9)	6.9 (6.1)
completeness (%)	98.2 (90.1)	97.1 (81.3)	99.5 (99.9)	84.2 (46.5)
[b]R_{merge}	0.094 (0.873)	0.070 (0.661)	0.088 (0.339)	0.039 (0.289)
[c]$R_{p.i.m}$	0.026 (0.278)	0.032 (0.356)	0.026 (0.101)	0.017 (0.128)
I/σ(I)	18.1 (2.5)	17.9 (2.2)	26.7 (5.6)	23.2 (4.6)
Anomalous correlation coef.		0.61 (-0.02)	0.68 (0.22)	0.38 (0.05)
Phasing Statistics from Xe dataset				
Isomorphous phasing power from (centric/acentric)	0.891/0.745			
Anomalous phasing power	0.752			
Figure of Merit (centric/acentric)	0.251/0.210			
Figure of Merit after DM	0.717			
Refinement Statistics				
[a]Resolution (Å)	40-3.7 (3.74 – 3.70)			
Working set reflections	45,569 (1,346)			
Test set reflections	5,070 (143)			
[d]R_{cryst} (%)	0.310 (0.480)			
[d]R_{free} (%)	0.347 (0.508)			
Average B factor (Å^2)	172			
Rmsd bond length (Å)	0.023			
Rmsd bond angle (°)	2.78			
Ramachandran plot (most favored, additional allowed, generously allowed, outliers)[h]	91.0%, 7.1%, 1.2%, 0.7%			

[a]Numbers in parentheses represent data in the highest resolution shell ().

[b]$R_{merge}(I) = \sum_{hkl}\sum_i |I_{hkl,i} - \langle I_{hkl}\rangle| / \sum_{hkl}\sum_i I_{hkl,i}$.

[c]$R_{p.i.m.}$ is the precision indicating merging R-factor (*S23*), with N = redundancy and

$$R_{p.i.m} = \sum_{hkl}[1/(N-1)]^{1/2}\sum_i |I_{hkl,i} - \langle I_{hkl}\rangle| / \sum_{hkl}\sum_i I_{hkl,i.}$$

[d]$R_{cryst} = \sum_{hkl} \| F_{obs}| - |F_{calc} \| / \sum_{hkl}|F_{obs}|$, calculated for the working set reflections. R_{free} was computed identically, except for the 10% of the reflections in the test set.

[e]collected on SSRL beam line 11-1

[f]collected on SSRL beam line 9-2

[g]collected on ALS beam line 8.2.1

[h]assigned with PROCHECK (*S24*)

Table S2 Data Processing, Phasing and Refinement Statistics for KI soaked MetN-C2

Space group	P 3_1 2 1
Unit cell dimensions (a, b, c)	53.28 Å, 53.28 Å, 150.50 Å
Wavelength (Å)	1.5418[e]
[a]Resolution (Å)	46 - 2.10 (2.21-2.10)
Unique reflections	14,838 (1,829)
Redundancy	19.2 (13.1)
Completeness (%)[1]	97.6 (85.0)
[b]R_{merge}	0.053 (0.082)
[c]$R_{p.i.m.}$	0.018 (0.032)
I/σ (I) [1]	47.7 (27.5)
Anomalous correlation coefficient	0.90 (0.72)
Phasing statistics	
[a]Resolution (outer shell)	20.0-2.1 (2.39-2.1)
Anomalous phasing power	1.4 (1.2)
Cullis R factor	0.55 (0.58)
Figure of Merit	0.43 (0.42)
Refinement statistics	
Resolution (Å)	44.1 – 2.1 (2.155-2.1)
Working set reflections	14,058 (823)
Test set reflections	731 (44) 5%
Number of atoms (protein, water, iodide)	1,570; 242; 11
[d]R_{cryst}	0.193 (0.149)
[d]R_{free}	0.254 (0.302)
Average B (Å^2)	18.1
Rmsd bond lengths (Å)	0.024
Rmsd bond angles (º)	1.94
Ramachandran plot (most favored, additional allowed, generously allowed, outliers)[f]	91.4%, 8.6%, 0%, 0%

[a]Numbers in parentheses represent data in the highest resolution shell ().

[b]$R_{merge}(I) = \sum_{hkl}\sum_i |I_{hkl,i} - \langle I_{hkl}\rangle| / \sum_{hkl}\sum_i I_{hkl,i}$.

[c]$R_{p.i.m.}$ is the precision indicating merging R-factor (*S23*), with N = redundancy and

$$R_{p.i.m} = \sum_{hkl}[1/(N-1)]^{1/2} \sum_i |I_{hkl,i} - \langle I_{hkl}\rangle| / \sum_{hkl}\sum_i I_{hkl,i.}$$

[d]$R_{cryst} = \sum_{hkl} \| F_{obs}| - |F_{calc} \| / \sum_{hkl}|F_{obs}|$, calculated for the working set reflections. R_{free} was computed identically, except for the 5% of the reflections in the test set.

[e]collected on a Rigaku MicroMax-007HF Microfocus, R-axis IV system

[f]assigned with PROCHECK (*S24*)

Supporting Online Material Figure Legends

Supporting Online Material Figure S1: Stereoview of the electron density map covering the MetNI transporter at 3.7 Å resolution, calculated with experimental phases from the single isomorphous replacement and anomalous scattering data of a xenon derivative, followed by solvent flattening and non-crystallographic symmetry averaging using the final refined operators. The electron density is contoured at 1 time the standard deviation of the map. The structure figures in the Supporting Online Material were prepared with MOLSCRIPT and RASTER3D *(S25, S26)*.

Supporting Online Material Figure S2: Stereoview of a binding site for selenomethionine near the dimer interface between the C2-domains of MetNI. The two subunits are differentiated by light green and purple bonds, respectively. The sidechain positions reflect the conformations observed in the 2.1 Å resolution structure of the isolated MetN-C2 domains, following adjustment and refinement to fit the MetNI density. The gray surface represents the electron density of an anomalous difference Fourier map calculated from diffraction data measured at the selenium edge from selenomethionine soaked crystals. The map was calculated at 5.2 Å resolution and contoured at 12 times the standard deviation of the electron density.

Supporting Online Material Figure S3: Dependence of the ATPase-rate of wildtype MetNI transported (solubilized in the detergent DDM) on the concentration of MgATP. The K_m and V_{max} obtained from the fit of this data to a Michaelis-Menten equation are 337 μM and 45.9 moles Pi/min/mole transporter; the curve calculated with these values is displayed. The error bars represent the standard deviations calculated from 4 measurements. ATPase activity is determined from the rate of phosphate release as monitored by the assay of Webb (*S17*).

Supporting Online Material Figure S4: Multiple structure alignment of the membrane spanning subunits MetI, ModB (PDB ID 2ONK), MalF and MalG (PDB ID 2R6G) using the program MUSTANG (*S21*). Helical elements are designated by the bar under the associated sequences, with the membrane spanning and extra-membrane helices denoted by black and red shading, respectively.

Supporting Online Material Figure S5: Stereoview of the relationship between TM2-TM4 from one membrane spanning subunit of the methionine (brown), molybdate (green) and maltose (MalG) transporters, following superposition of the other subunit onto the corresponding helices of MalF. The yellow and red lines denote the rotation axes corresponding to the dominant transformation in a principal components analysis (*S22*) of the membrane spanning (yellow axis) and ABC (red axis) subunits, respectively. Relative to the MalG subunit, the rotations about the yellow axis for the corresponding membrane spanning subunits of the molybdate and methionine transporters are ~20˚ and ~32˚, respectively; for the ABC subunits attached to the counterpart of MalF, the corresponding rotations about the red axis are ~25˚ and ~31˚ for the molydate and methionine transporters, respectively. For clarity, only the β-strand and α-helix surrounding the P-loops of the ABC subunits are illustrated as coils.

FigS1

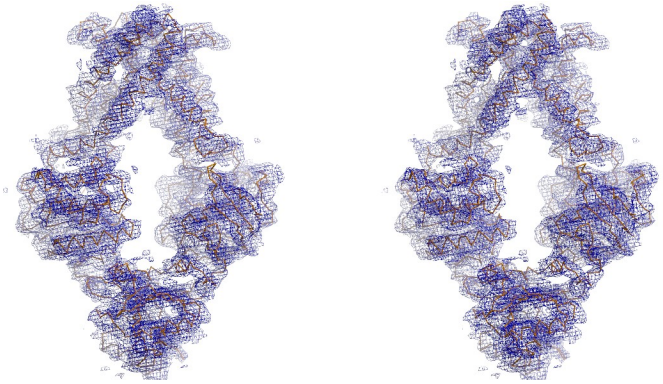

FigS2

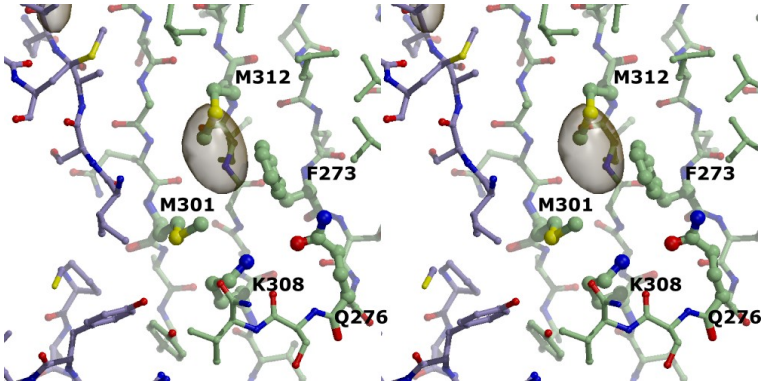

FigS3

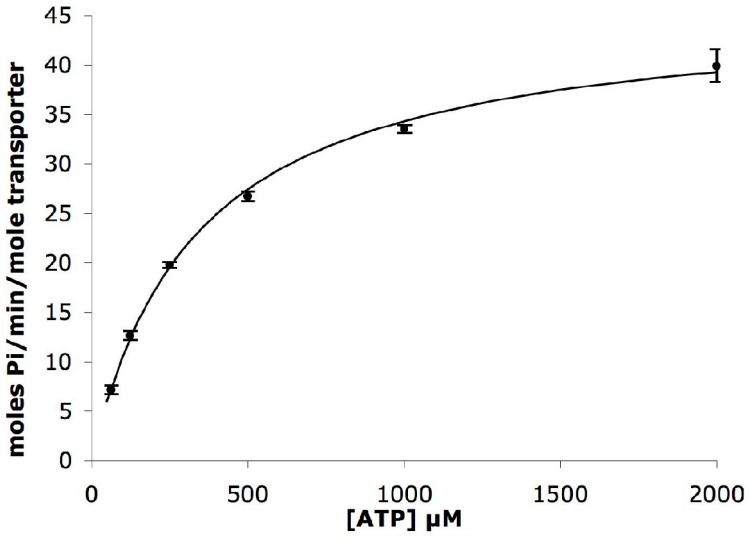

FigS4

```
2ONK-C      43                                    SDP      AVWKVVLTTYYAALISTLIAVIFGTPL
2R6G-F     242 ANWGDEKLS  PGYTVTTGWKNFTRVFTDEGIQKPFLAIFWWTVVFSLITVFLTVAVGMVL
2R6G-G      74             ITPPP                          FPVLLWLWNSVKVAGISAIGIVALSTTC
METI-A       8                                            LLVRGVWETLAMTFVSGFFGFVIGLP
```

```
2ONK-C      73 AYIL             ARKSFPGKSVVEGIVDLPVVIPHTVAGIALLVVFGS  SGLIGSF
2R6G-F     303 ACLV             QWEALRGKAVYRVLLILPYAVPSFISILIFKGLFNQSFGEINMMLS
2R6G-G     107 AYAF             ARMRFPGKATLLKGMLIFQMFPAVLSLVALYALFD    R LGE
METI-A      34 VGVLLYVTRPGQII   ANAKLYRTVSAIVNIFRSIPFIILLVWMIPFTR    V
```

```
2ONK-C     120   SPL     KFVD   ALPGIVVAMLFVSVPIYINQAKEGFASVDVRLEHVARTLGSSPL
2R6G-F     353 ALFGVKPAWFSDPTTARTMLIIVNTWLGYPYMMILCMGLLKAIPDDLYEASAMDGAGPF
2R6G-G     150  YIPF      IGLN   THGGVIFAYLG GIALHVWTIKGYFETIDSSLEEAAALDGATPW
METI-A      82   IVG       TSI   GLQAAIVPLTVGAAPFIARMVENALLEIPTGLIEASRAMGATPMQ
```

```
2ONK-C     171   RVFFTVSLPLSVRHIVAGAIMSWARGISEFGAVVVIAYY                PM I
2R6G-F     412   QNFFKITLPLLIKPLTPLMIASFAFNFNNFVLIQLLTNGGPDRLGTTTPA  GYTD L
2R6G-G     201   QAFRLVLLPLSVPILAVVFILSFIAAITEVPVASLLL                RDVNSY T
METI-A     133 IV    RKVLLPEALPGLVNAATITLITLVGYS    AMGG                 AVGAGG
```

```
2ONK-C     213 APTLIYERYLSE     GLSAAMPVAAILILLSLAVFVALRIIVG                252
2R6G-F     467 LVNYTYRIAFEGGGGQDFGLAAAIATLIFLLVGALAIV                      504
2R6G-G     245 LAVGMQQYLN   PQNYLWGDFAAAAVMSALPITIVFLLAQRWLVNGLTAGGVKG    296
METI-A     172 LGQIGYQYGYIG     YNAAVMNTVLVLLVILVYLIQFAGD                  208
```

FigS5